Robotica (2006) volume 24, pp. 11–21. © 2005 Cambridge University Press
doi:10.1017/S026357470500189X Printed in the United Kingdom

Tactile tele-operation of a mobile robot with a collision vector

Jae-Pyung Ko and Jang-Myung Lee*

Department of Electronics Engineering, Pusan National University, Pusan 609-735 (South Korea)

(Received in Final Form: March 21, 2005)

SUMMARY

In this paper, we have developed and implemented a system that combines autonomous obstacle avoidance with force-reflective tele-operation. In this system, a tele-operated mobile robot is controlled by a local two-degrees-of-freedom force-reflective joystick that a human operator holds while he is monitoring the screen. The force-reflective joystick transforms the relation between a mobile robot and the environment to the operator as a virtual force. A virtual force is generated in the form of a new collision vector and reflected to the operator, which makes the tele-operation of a mobile robot safe from collision in an uncertain and obstacle-cluttered remote environment. A mobile robot controlled by a local operator usually takes pictures of remote environments and sends the images back to the operator over the Internet. Because of limitations of communication bandwidth and the narrow view-angles of the camera, the operator cannot observe shadow regions and curved spaces. To overcome this problem, a new form of virtual force is generated along the collision vector according to both distance and approaching velocity between an obstacle and the mobile robot, which is obtained from ultrasonic sensors. This virtual force is transferred back to a master (two degrees of freedom joystick) over the Internet to enable a human operator to feel the geometrical relation between the mobile robot and the obstacle. It is demonstrated by experiments that this haptic reflection improves the performance of a tele-operated mobile robot significantly.

KEYWORDS: Tele-operation; Collision Vector; Force Reflection; Virtual Impedance; Teleautonomous System.

I. INTRODUCTION

The conventional tele-operation of mobile robots relies on visual contact with the operator, either directly or through video transmissions. Under such conditions, a human tele-operator must exercise extreme care, especially in obstacle-cluttered environments. Consequently, the actual traveling speed of the mobile robot might be very slow. When dust, smoke, or steam inhibit vision based guidance, conventional tele-operated activity is ruled out altogether. A teleautonomous system, which is explained in a previous study,[1] can overcome this problem, that combines autonomous obstacle avoidance with tele-operation. In this system, the tele-operator can guide the mobile robot even without any visual contact. The mobile robot follows the general direction prescribed by the operator. When the robot encounters an obstacle, it autonomously avoids collision with that obstacle, trying to match the operator's prescribed direction as close as possible.

Telepresence is the ultimate factor in reliable and skillful tele-operations. If all the information at a remote site can be transferred to a human operator in real time, telepresence can be achieved naturally. In a reliable tele-operation system, bilateral control, in which information at the remote and operator sites is shared together, is generally utilized. In most cases of bilateral tele-operations, position information is reflected to the operator as images while the operator is holding a joystick for the generation of motion commands. However, this visual information is not always sufficient. For example, when a mobile robot enters a tunnel, the capturing of environmental images is delayed for a few seconds.

As explained in the previous studies,[2–5] one of the general trends in reliable tele-operation is to generate a virtual force between a robot and the environment, which, in addition to the visual information, is transferred to a human operator through a joystick as tactile information.[4] Among the studies of tele-operated mobile robots which seriously investigate collisions between mobile robots and obstacles, there are not many studies that focus on bilateral control using force reflection.[5]

In this paper, we have developed a system that combines autonomous obstacle avoidance with force-reflective tele-operation. In this system, a tele-operated mobile robot is controlled by a local two-degrees-of-freedom force-reflective joystick that a human operator holds while he is monitoring the screen. The force-reflective joystick transforms the relation between a mobile robot and the environment to the operator as a virtual force. As shown in Fig. 1, a bilateral tele-operation system consists of an operator, a joystick, a communication block, and a mobile robot. The virtual force from a mobile robot, which is a function of the distance and relative velocity between a mobile robot and an obstacle, is reflected to the joystick as a force between the joystick and the human hand using two motors in the joystick. Therefore, the operator can feel, and avoid, collisions through the haptic joystick in spite of the limitations in visual display, which are transmission delay, limited bandwidth, bad illumination, occulusion, and camera distortions.

To generate the virtual force, the relation between a mobile robot and an obstacle, and to guide autonomous operation of mobile robot is modeled as a virtual mass-spring-damper, that

* Corresponding author. E-mail: jmlee@pusan.ac.kr

https://doi.org/10.1017/S026357470500189X Published online by Cambridge University Press

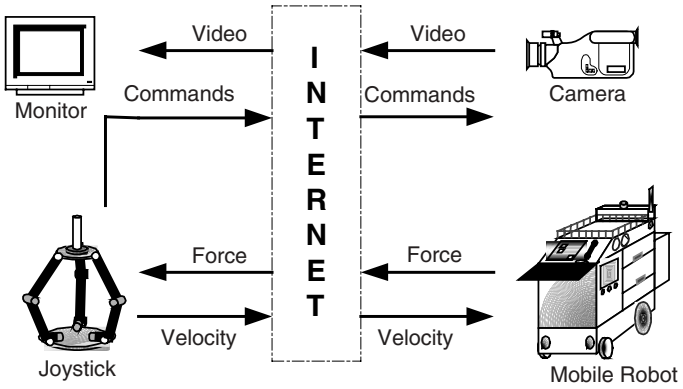


Fig. 1. Block diagram of the tele-operation system.



Fig. 3. 2DOF joystick system.

is, an impedance. The virtual impedance method considering the approach velocity to an obstacle seems to be more suitable than the conventional potential field methods, since it has the capability to cope with moving obstacles. However, the obstacle avoidance strategy should be properly modified for the different shapes of the obstacles. As a major contribution of this study, a collision vector is newly defined from the ultrasonic sensor data, which is normal to the obstacle. Through the experiments, the effectiveness of the collision vector in avoiding local minima is demonstrated.

II. SYSTEM MODEL

A bilateral tele-operation system is composed of a human operator, a joystick, a Global Path Planner (GPP), a remote PC, a mobile robot and a communication block, as shown in Fig. 2. If a human operator exerts force F_h to the joystick, the displacement of the joystick is generated as X_m. Based on the data, the GPP generates the optimal trajectory for the mobile robot to the goal, and transfers the data to a Dynamic Avoidance Planner (DAP) that makes the robot follow the given trajectory while avoiding the obstacles. That is, the GPP (local PC) creates X_d and V_d according to the X_m, and transfers them to the remote PC through the Internet. When the slave mobile robot receives X_d and V_d from the remote PC through a wireless LAN, the DAP of the mobile robot generates $\ddot{x}_s$ according to X_d, V_d, and the data from ultrasonic sensors. Then, $\ddot{x}_s$ is transferred to the servo-driver that generates **u** and $\boldsymbol{\omega}$ (the control inputs of a mobile robot) to track the given path.

With this system architecture, the operator at the local site can feel the telepresence by means of the feedback data that are composed of the repulsive force, F_b, between the mobile robot and obstacles, and the visual information, I.

II.1. Master (joystick) system model

A human operator can feel the virtual force generated between a tele-operated mobile robot and the remote environment through the two-degrees-of-freedom joystick as shown in Fig. 3.

Figure 4 shows the block diagram of a joystick system. To control the joystick, which basically generates motion commands, a joystick controller was designed using an 80C196KC microprocessor. This joystick also retrieves the force data F_b that is sent from the remote PC to the operator. For this retrieval, two axial motors are driven by PWM (Pulse Width Modulation) outputs corresponding to the F_b. L298N DC motor drives are used to amplify the power. The position of the joystick is measured by potentiometers connected to each axis. An A/D (Analog to Digital) converter transforms the voltage measured by the potentiometers into 10-bit digital data that are reflected to the joystick controller as inputs. To measure the force at the joystick held by an operator, a current sensor is used. The current through the sensor is transformed into voltage by a 2Ω resister and passed through an LPF (Low Pass Filter). The resultant voltage is converted into 10-bit

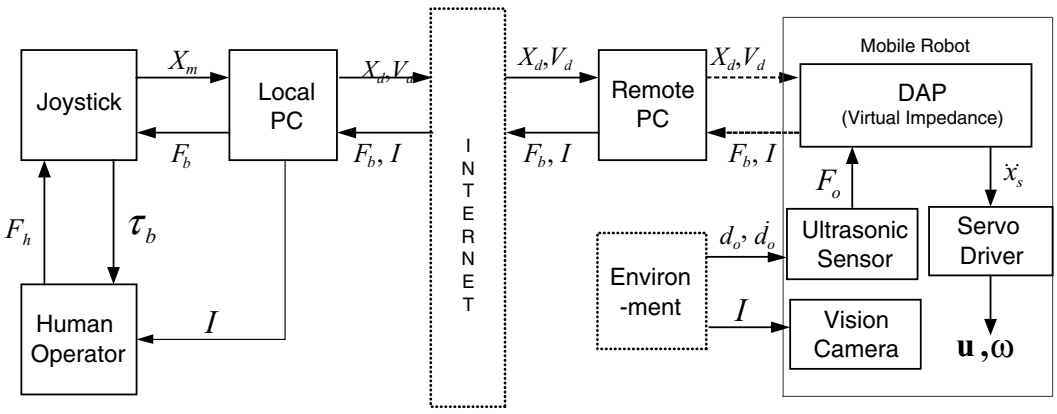


Fig. 2. Tele-operation system architecture.

https://doi.org/10.1017/S026357470500189X Published online by Cambridge University Press

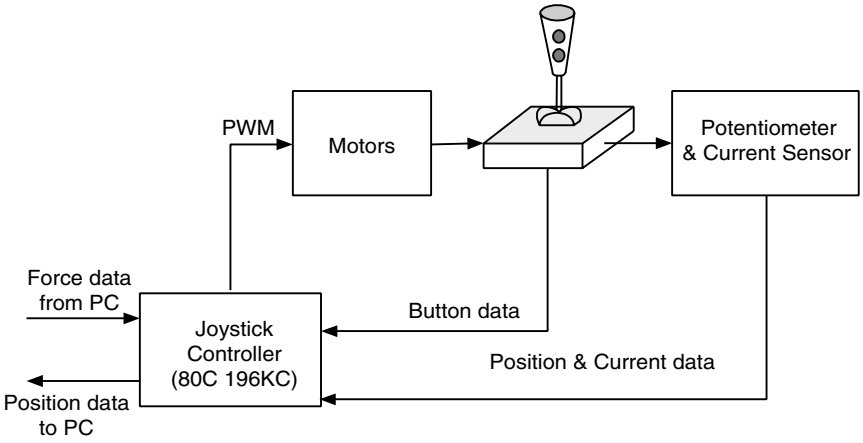


Fig. 4. Block diagram of a joystick system.

digital data by the A/D converter. The digital data are also delivered to the joystick controller as control inputs.

Human operator's commands. When the operator exerts force F_h to the joystick, this forceF_h creates the joystick displacement X_m. When the x-axis is aligned to the heading of the mobile robot, X_m generates the desired velocity V_d and the desired position X_d of the robot as follows:

$$V_d(t) = K_m \cdot X_m(t) \tag{1}$$

$$X_d(t) = \int_0^{T_3} K_v \cdot V_d(t) \cdot dt \tag{2}$$

where $X_m = \left[\begin{smallmatrix} X_{mx} \\ X_{my} \end{smallmatrix}\right]$, $X_d = \left[\begin{smallmatrix} X_{dx} \\ X_{dy} \end{smallmatrix}\right]$, $V_d = \left[\begin{smallmatrix} V_{dx} \\ V_{dy} \end{smallmatrix}\right]$, K_m and K_v are scaling constants, and T_3 is the sampling time for the GPP.

Virtual force feedback. The virtual force F_b reflected to the operator is represented as

$$F_b = \sum_{i=0}^{n} F_{ot}(t) \tag{3}$$

where n is the number of obstacles.

The F_b which is generated from a mobile robot at a remote site, is transferred to the operator at the master site as

$$\tau_b(t) = \text{sat}(K_b \cdot F_b(t)) \tag{4}$$

$$\text{sat}(x) = \begin{cases} x, & if\,|x| \le x_{\max} \\ \text{sign}(x) \cdot x_{\max}, & \text{otherwise} \end{cases} \tag{5}$$

where K_b is the force feedback gain constant. And the saturation function, *sat(x)*, is used so as to prevent the feedback force F_b from exceeding the driving power of the motor.

In spite of the limited information from the visual feedback, such as the transmission delay of a channel, the limitation of bandwidth, and the camera distortion, now the operator can recognize the geometrical relation between the robot and the objects realistically with the aid of the force τ_b felt from the joystick.

II.2. Slave (mobile robot) model

Figure 5 shows the configuration of the mobile robot used for this research. In the middle of the mobile robot, the sixteen ultrasonic sensors are attached at every 22.5° to acquire the distance data to the obstacles.

The state of mobile robot is represented as a vector $\mathbf{p} = [x\ y\ \theta]^T$ composed of position and orientation variables as shown in Fig. 6. In general, the motion of the mobile robot can be modeled by the translation velocity, **u**, and the angular velocity, ω.[6,7] The translation velocity, **u**, and angular velocity, ω are calculated using each encoder data of wheel and gyro sensor at each control period.

$$u = \frac{1}{2}(v_R + v_L) \tag{6}$$

$$\omega = \frac{1}{l}(v_R - v_L). \tag{7}$$

The velocity of mobile robot in the world coordinates is represented as a Jacobian matrix $J(p)$ according to input variable q. And position and orientation vector p is represented as a integral equation.

$$\dot{p} = J(p)\dot{q}$$

$$\begin{bmatrix} \dot{x} \\ \dot{y} \\ \dot{\theta} \end{bmatrix} = \begin{bmatrix} \cos\theta & 0 \\ \sin\theta & 0 \\ 0 & 1 \end{bmatrix} \begin{bmatrix} u \\ \omega \end{bmatrix} \tag{8}$$

$$p = \begin{bmatrix} x \\ y \\ \theta \end{bmatrix} = \begin{bmatrix} x_0 \\ y_0 \\ \theta_0 \end{bmatrix} + \begin{bmatrix} \int u(\tau)\cos(\theta(\tau))\,d\tau \\ \int u(\tau)\sin(\theta(\tau))\,d\tau \\ \int \omega(\tau)\,d\tau \end{bmatrix}. \tag{9}$$

Reference trajectory generation. A remote mobile robot implements the obstacle avoidance in real time according to the reference trajectory created by an operator. As illustrated in Fig. 7, $V_d(t)$ and $X_d(t)$ from the master are transformed into the robot coordinates and represented as $\dot{X}_r(t)$ and $X_r(t)$ which are

$$\begin{bmatrix} \dot{X}_{rx}(t) \\ \dot{X}_{ry}(t) \end{bmatrix} = \begin{bmatrix} \cos\theta & -\sin\theta \\ \sin\theta & \cos\theta \end{bmatrix} \begin{bmatrix} V_{dx}(t) \\ V_{dy}(t) \end{bmatrix} \tag{10}$$

https://doi.org/10.1017/S026357470500189X Published online by Cambridge University Press

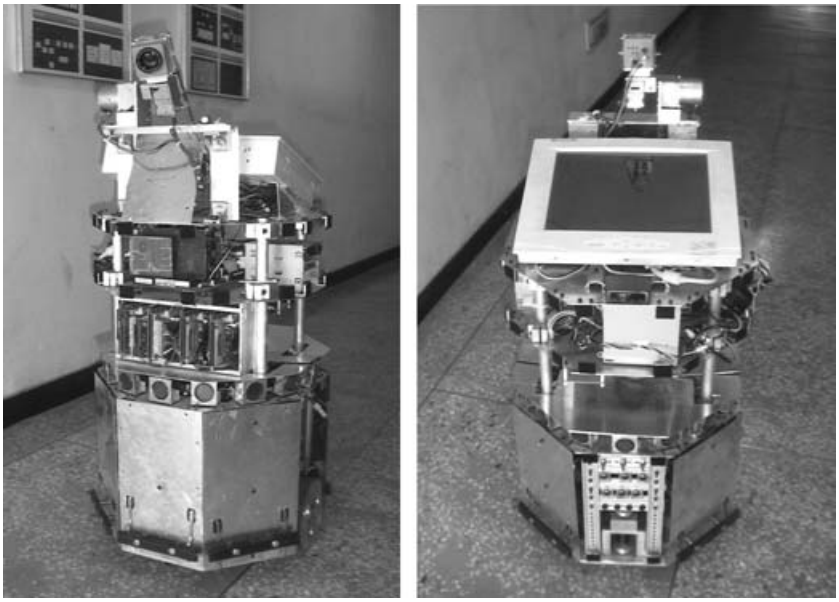


Fig. 5. The configuration of the mobile robot.

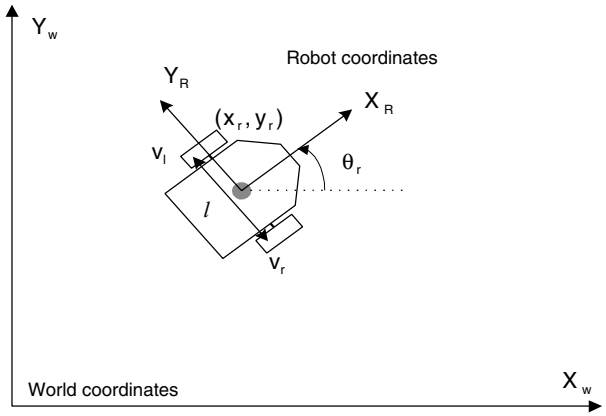


Fig. 6. A Mobile Robot Model.

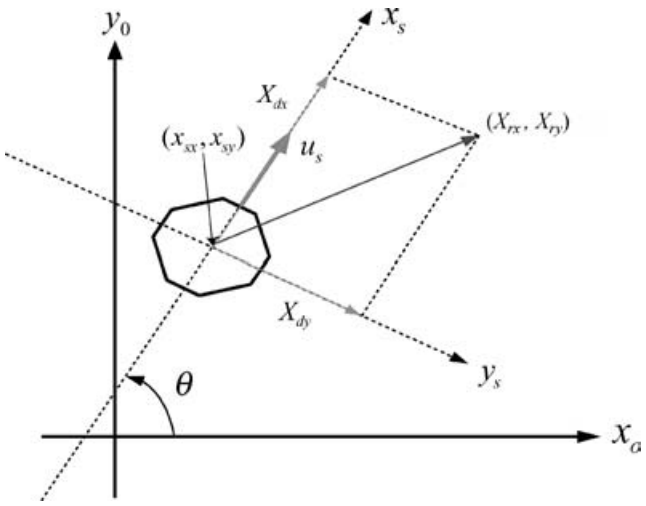


Fig. 7. Generation of reference trajectory.

and

$$\begin{bmatrix} X_{rx}(t) \\ X_{ry}(t) \\ 1 \end{bmatrix} = \begin{bmatrix} \cos\theta & -\sin\theta & x_{sx}(t) \\ \sin\theta & \cos\theta & x_{sy}(t) \\ 0 & 0 & 1 \end{bmatrix} \begin{bmatrix} X_{dx}(t) \\ X_{dy}(t) \\ 1 \end{bmatrix} \quad (11)$$

where (x_{sx}, x_{sy}) represents the current robot coordinates.

III. A NEW VIRTUAL IMPEDANCE ALGORITHM

As shown in Fig. 8, in the GPP, the human operator generates $X(t)$ and $\dot{X}(t)$ using the joystick, while in the DAP, the command to the servo driver, $\ddot{x}(t)$, is generated to track the given trajectory $X(t), \dot{X}(t)$ as well as to avoid obstacles based on the virtual impedance model. Before proposing a new virtual impedance algorithm, the related work is surveyed in order to provide a firm basis for this research.

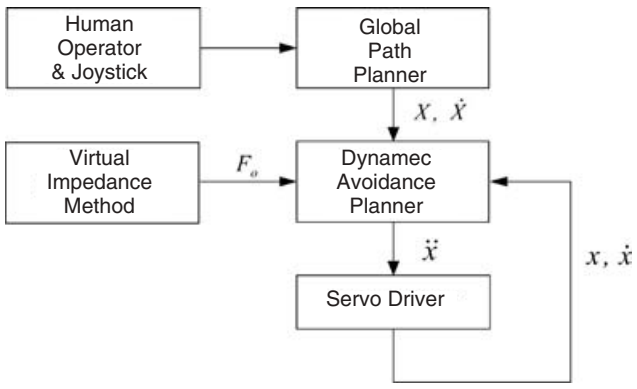


Fig. 8. Trajectory tracking and obstacle avoidance.

https://doi.org/10.1017/S026357470500189X Published online by Cambridge University Press

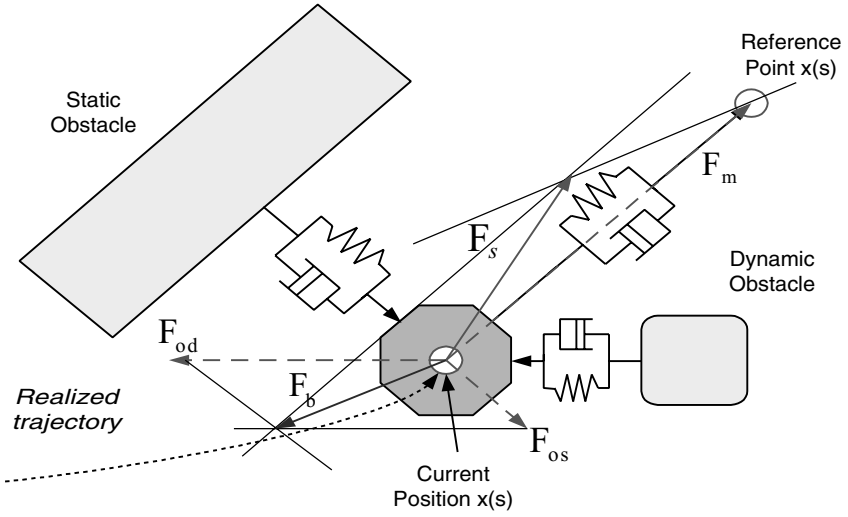


Fig. 9. Virtual impedance model.

III.1. Review of obstacle avoidance method

Approaches to obstacle avoidance are reviewed and discussed in view of their applicability to real-time obstacle avoidance.

Edge detection methods. A general and commonly employed method is based on edge-detection.[8] In this method, the algorithm tries to determine the vertical edges of the obstacle and consequently attempts to steer the robot around an edge. The line connecting the two edges is considered to represent one of the obstacle's boundaries. A disadvantage of the obstacle avoidance method based on the edge detection is that the robot needs to stop in front of the obstacle. Therefore it is not suitable for real-time obstacle avoidance.

Certainty grid methods. In the certainty grid world model,[9] the robot's work area is represented by a two-dimensional array of square elements denoted as cells. Each cell contains a CV (certainty value) that indicates the measure of confidence that an obstacle exists within the cell area. This method is not suitable for the real-time obstacle avoidance, since it requires a robot to stop in order to scan the work area, and also because it has a heavy computational load.

Potential field method. This method[10,11] achieves the collision avoidance motion planning of a robot by generating a virtual force against obstacles and toward the goal. That is, it generates an attractive force between the mobile robot and a target and generates a repulsive force against an obstacle that the mobile robot confronts in navigation. This method has the advantage of making the fast motion planning for nearby obstacles, but has a shortcoming of getting into a local minimum where the attractive and the repulsive forces are equal. To overcome this local minimum problem, the extended virtual force field method is proposed, where a free vector is added to the repulsive force. However the virtual force becomes larger for larger obstacles since the repulsive forces are coming from all obstacle-detecting sensors, which makes this method unsuitable for certain applications.

Virtual impedance method. Impedance control is an algorithm that adjusts the relation between a velocity command and contact force, which models the interconnection between an uncertain environment and a robot as an impedance.[12] In the virtual impedance method,[13,14] the impedance is used to generate a repulsive force for the navigation of a mobile robot in avoiding collisions with obstacles. As shown in Fig. 9, the virtual impedance method generates a virtual force according to the distance and relative velocity between the robot and an obstacle, which can be modeled as a spring and a damper. F_o consists of repulsive forces against a static obstacle, F_{os}, and a dynamic obstacle, F_{od}. Obstacle avoidance is handled generally in the DAP, while the GPP generates the trajectory $X(t)$, $\dot{X}(t)$ according to the joystick output, X_m.

Virtual impedance can be defined as the following procedures. First of all, the acceleration for the mobile robot can be represented as

$$\ddot{x}_s = \frac{1}{M_s}\left\{F_m + \sum_{i=0}^{n} F_{oi}\right\} \tag{12}$$

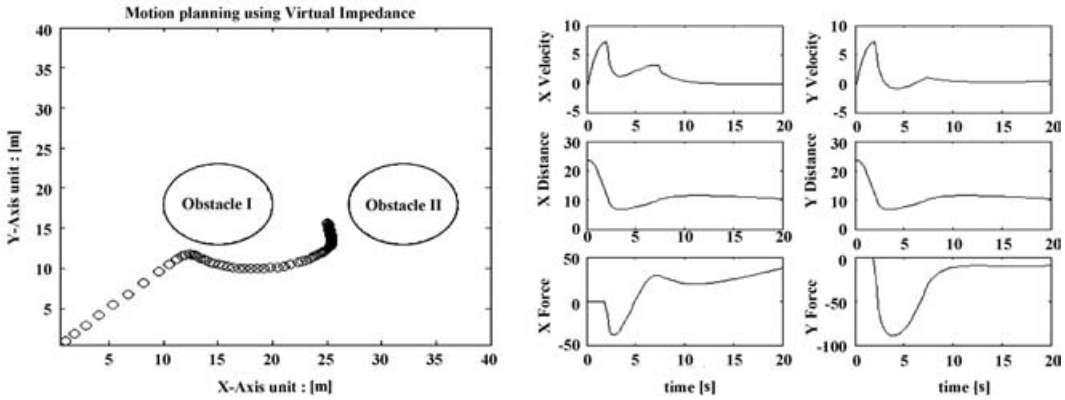
where F_m is the attractive force generated between the current position of the robot and the reference point generated by the master, and F_{oi} is the virtual repulsive force between the current robot and a nearly i_{th} obstacle among n objects. Note that the virtual mass M_s does not represent the real "mass" of the robot but the relative rigidity of the robot trajectory.

The attractive force, F_m, is generated as

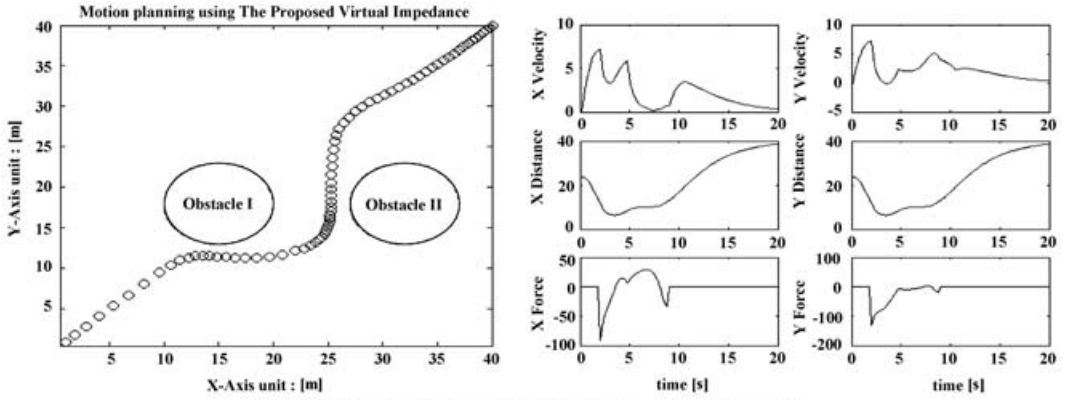
$$\begin{aligned} F_m &= K_r(X_{rs}) + D_r(\dot{X}_{rs}) \\ &= -K_r(x_s - X_r) - D_r(\dot{x}_s - \dot{X}_r) \end{aligned} \tag{13}$$

where x_s is the present position of the robot, and X_r is the reference point of the robot at the present time (planned by the GPP). And K_r and D_r are a spring and a damper constant between the robot and the reference point, respectively.

https://doi.org/10.1017/S026357470500189X Published online by Cambridge University Press



(a). With a conventional virtual impedance method in case of a static obstacle.



(b). With a new virtual impedance method in case of a static obstacle.

Fig. 10. Motion planning with $K_r = 2$, $D_r = 10$, $K_o = 10$, $D_o = 15$, and $M_s = 10$.

The summation of virtual repulsive force can be expressed as

$$F_o = K_o(X_{so}) + D_o(\dot{X}_{so}) = \sum_{i=0}^{n} \{K_o(x_s - x_{oi})^{-1} + D_o(\dot{x}_s - \dot{x}_{oi})\} \quad (14)$$

where K_o and D_o are a spring and a damper constant between the robot and the obstacle, respectively, and x_{oi} and $\dot{x}_{oi}$ are the position and the velocity of the ith obstacle, respectively. And n is the number of obstacles within the sensing area of the robot.

Actually, the feedback force F_b between the human hand and the joystick, which is physically the same as F_o, is maintained as a constant unless the operator moves the joystick to change the trajectory.

III.2. A new virtual impedance method

The virtual impedance method considering the approach velocity to an obstacle seems to be more suitable than the conventional potential field methods, since it has the capability to cope with moving obstacles. However, the obstacle avoidance strategy should be properly modified for the different shapes of the obstacles. For example, when the relative velocity between a mobile robot and an obstacle generates a repulsive force, the mobile robot cannot even approach near to the narrow channel, which is shown by the simulation in Fig. 10(a).

In this paper, therefore, we propose a new virtual impedance method that sets a damper as the rate change of the shortest distance between a mobile robot and an obstacle. The new proposed virtual impedance model is defined as

$$F_o(s) = K_o(X_{s,o}(s)) + D_o(\dot{X}_{s,o}(s)) = \begin{cases} \sum_{i=0}^{n} \left\{ K_o(\rho_0 - \|d_i\|)\frac{d_i}{\|d_i\|} - D_o(\Delta(d_i))\frac{d_i}{\|d_i\|} \right\}, & \text{when } \|d_i\| < \rho_0 \\ 0, & \text{otherwise} \end{cases} \quad (15)$$

where d_i is the shortest vector to the obstacle, $\Delta(d_i) = d_i[t] - d_i[t-1]$, and ρ_o is the measurable range of an ultrasonic sensor and the simulation result is shown in Fig. 10(b). Fig. 11 shows the simulation result of motion planning with virtual impedance method in case of a moving obstacle and the same parameters in Fig. 10.

Detection of a collision vector for an obstacle. The shortest vector to the obstacle is renamed as a collision vector that can be obtained practically using the ultrasonic sensors. That is, we are going to define a normal vector to the tangential line of an obstacle as a collision vector. In the experimental robot, there are sixteen 6500-series ultrasonic sensors from Polaroid Corp. to acquire the distance data between a mobile robot and obstacles. In real experiments, we cannot obtain accurate distance data in cases where the angle between a normal vector to a tangential line of an object and the beam

https://doi.org/10.1017/S026357470500189X Published online by Cambridge University Press

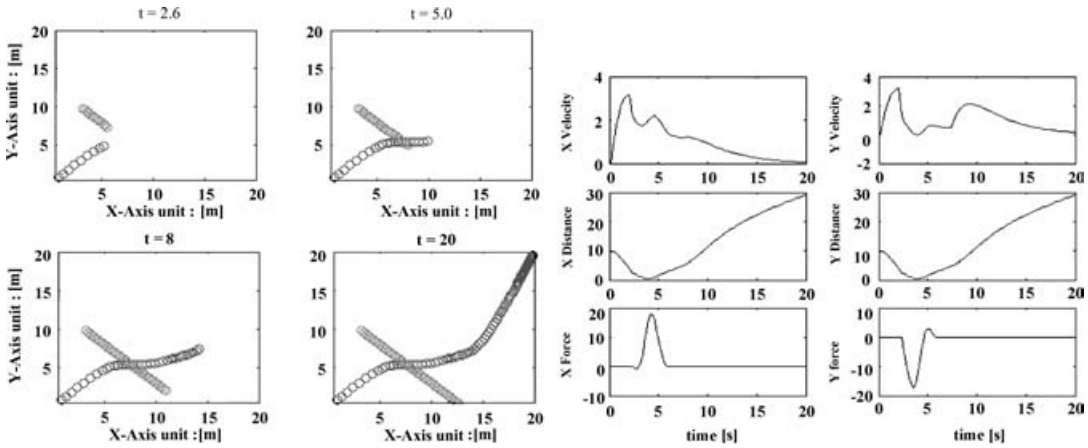


Fig. 11. Motion planning with virtual impedance method in case of a moving obstacle. (@$K_r = 2,\ D_r = 10,\ K_o = 10,\ D_o = 15$, and $M_s = 10$).

of an ultrasonic sensor is more than 30 degrees. This is caused by poor directionality, specular reflections and frequent misreadings of ultrasonic sensors, and limits the effective number of sensors for the collision vector decision to three, since there is an ultrasonic sensor every 22.5 degrees.

To generate the virtual repulsive force to avoid an obstacle that might be invisible, the collision vector for the obstacle needs to be obtained by using the ultrasonic sensors. Supposing that a mobile robot is moving in a building, the shape of obstacles can be classified as a cylinder (including a person) or a plane (a wall, a corner, *etc*). Therefore, with the ultrasonic sensors arranged in a circular pattern every 22.5 degrees, three cases of collision vectors shown in Fig. 12 may include all the possibilities of the relation between the robot and the obstacle.

a. Case 1. A small cylindrical obstacle which could be a person is detected by only one ultrasonic sensor. In this case, the collision vector, $\overrightarrow{C}$, can be obtained directly by

$$\overrightarrow{C} = -\overrightarrow{L_{\min}}. \tag{16}$$

b. Case 2. An obstacle is detected by two neighboring ultrasonic sensors. In this case, first of all, we define the shorter distance vector as $\overrightarrow{L_{\min}}$. The other distance vector is defined as $\overrightarrow{L_R}$ in the case that it is to the right of $\overrightarrow{L_{\min}}$. Using the points P_L, P_R, the lines $\overrightarrow{L_L}$, $\overrightarrow{L_R}$, and the tangential line of the obstacle, $\overline{P_L P_R}$, can be obtained. And the normal vector to this line across the point P_s, that is, the collision vector, $\overrightarrow{C}\ (=\overrightarrow{P_o P_s})$, can be calculated to obtain the point P_o as

$$\overrightarrow{C} = \overrightarrow{P_o P_s} \tag{17}$$

$$P_o = (x_o, y_o) = \left(\frac{V \cdot x_L - y_L}{V + \frac{1}{V}}, -\frac{-x_L + \frac{1}{V} y_L}{V + \frac{1}{V}} \right) \tag{18}$$

where $V = \frac{y_L - y_R}{x_L - x_R}$.

c. Case 3. An obstacle is detected by three neighboring ultrasonic sensors. At first, the shortest distance vector among the three detected distance vectors is defined as $\overrightarrow{L_{\min}}$. Then, by the same procedure as in Case II, $\overrightarrow{C}$ can be calculated by Eq.'s (17) and (18). Note that $\overrightarrow{L_e}$ is an unreliable datum, because the angle between $\overrightarrow{L_e}$ and $\overrightarrow{C}$ is over 30 degrees. Therefore, the collision vector, $\overrightarrow{C}$, can be obtained using only three distance vectors, $\overrightarrow{L_{\min}}$, $\overrightarrow{L_L}$ and $\overrightarrow{L_R}$.

Using $\overrightarrow{C}$, acquired above, the virtual impedance model proposed in Eq. (15) can be modified according to

$$F_o(s) = K_{s,o}(X_{s,o}(s)) + D_{s,o}(\dot{X}_{s,o}(s))$$

$$= \begin{cases} \sum_{i=0}^{n} \{K_{s,o}(\rho_0 - \| \overrightarrow{C} \|) \overrightarrow{C}_{unit} - D_{s,o}(\Delta \| \overrightarrow{C} \|) \overrightarrow{C}_{unit}\}, & \text{when } \| \overrightarrow{C} \| < \rho_0 \\ 0, & \text{otherwise.} \end{cases} \tag{19}$$

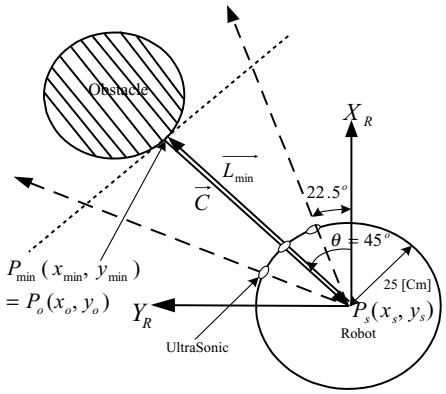
IV. SIMULATIONS AND EXPERIMENTATION

IV.1. Simulations

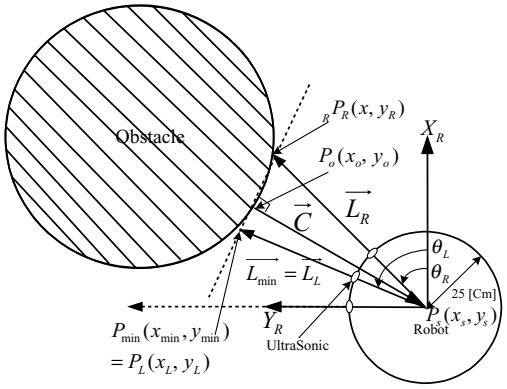
First of all, the effectiveness of a collision vector in obstacle avoidance is demonstrated through simulations. Figure 10(a) is the simulation result using the conventional virtual impedance model defined in Eq. (14). Each small circle represents the location of the mobile robot at the k_{th} instance. The mobile robot is programmed to move from the left-bottom corner to the right-top goal while avoiding two obstacles in the middle of the reference trajectory. A large time delay or time slack is caused by the defined damper around obstacles, and the mobile robot is finally blocked at the center of two nearby obstacles. Figure 10(b) is a simulation result of the proposed impedance model defined in Eq. (19). The damper causes the deceleration of the mobile robot before a collision and prevents the mobile robot from deviating from the programmed path after obstacle avoidance. Note that in the middle of the two obstacles, two collision vectors are generated, which become the bases for the repulsive forces mostly cancelled out by each other. At that moment, the attraction force to the goal plays the major role in guiding the mobile robot.

Note that in the tele-operation of a mobile robot with the conventional virtual impedance method, the robot may collide with a human in a corridor due to a large repulsive

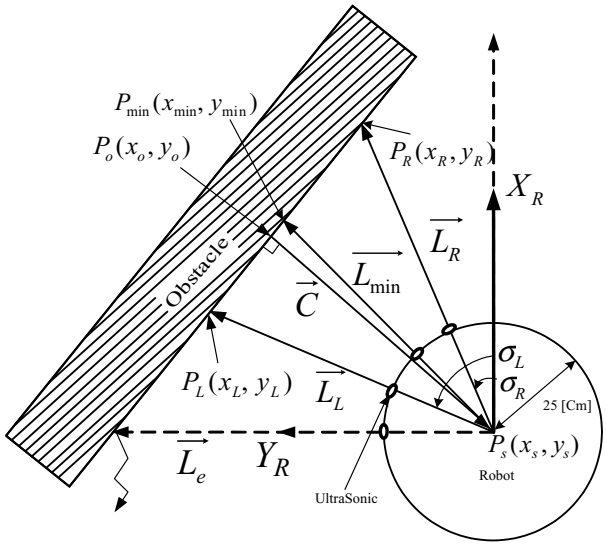
https://doi.org/10.1017/S026357470500189X Published online by Cambridge University Press



(a) Case I.



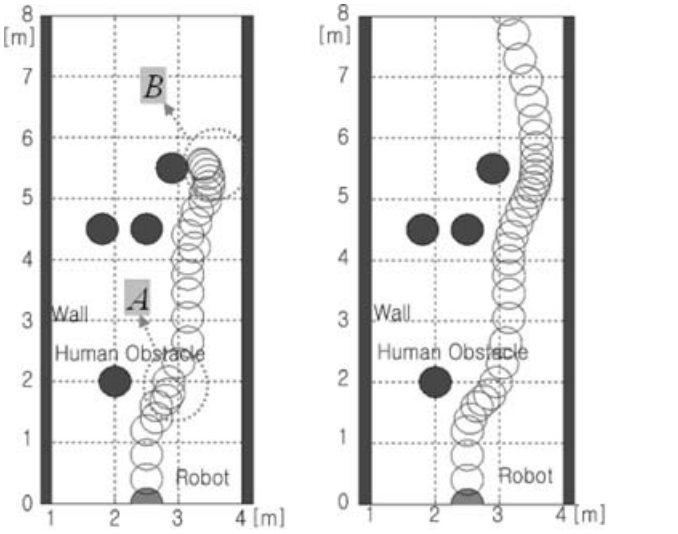
(b) Case II.



(c) Case III.

Fig. 12. Collision vector against an obstacle.

force for avoiding a wide wall, which becomes very large since all the repulsive forces from the wall-detecting sensors are combined. However, in this new scheme, the repulsive force from the nearby human is bigger than that from the wall since only a collision vector generates the repulsive force for each obstacle.



(a) Conventional PFM. (b) Proposed collision vector method

Fig. 13. Comparison of the PFM and the proposed method.

Now further simulations are performed to verify the superiority of this new virtual impedance-based obstacle avoidance scheme to the PFM. Figure 13(a) shows the case in which the virtual repulsive force becomes large for a wide wall according to the conventional PFM, while (b) shows the case in which the virtual repulsive force is generated by a collision vector for obstacle avoidance. Through a comparison of these two cases, the following can be concluded. In case (a), there is an oscillation of the mobile robot around point A. It is caused by the change of the sensor that detects the obstacle, which changes the sum of the repulsive force. Also, it suffers from a collision at point B by ignoring the repulsive force against a small obstacle such as a human compared with a large obstacle such as a wide wall. The simulation results show that with the PFM, the repulsive force of a small obstacle can be over-looked by that of a large obstacle. However, there does not exist any oscillation or collision in case (b), which is the result of the new obstacle avoidance.

IV.2. Experimentation

The operator at the local site can control the robot at the remote site by using the client program over the Internet, as shown in Fig. 14.

The operator generally recognizes the remote environment with the vision data. However, he cannot recognize under certain circumstances his view of the remote environment is limited on account of the narrow view-angle of the camera, the limitation of communication bandwidth, and the lack of lighting. The sampling time for the GPP, T_3, is set to be greater than or equal to the sampling time of the DAP, $T_2 = 250[ms]$. And the sampling time for the servo driver is $T_1 = 50[ms]$ as shown in Fig. 15. In this study, time delay problem such as the transmission delay of a velocity and position command in the Internet environment, is not considered. When a human operator controls the joystick, the motion command is generated. And it is transferred to the remote slave robot every 250 ms according to the direction of joystick

https://doi.org/10.1017/S026357470500189X Published online by Cambridge University Press

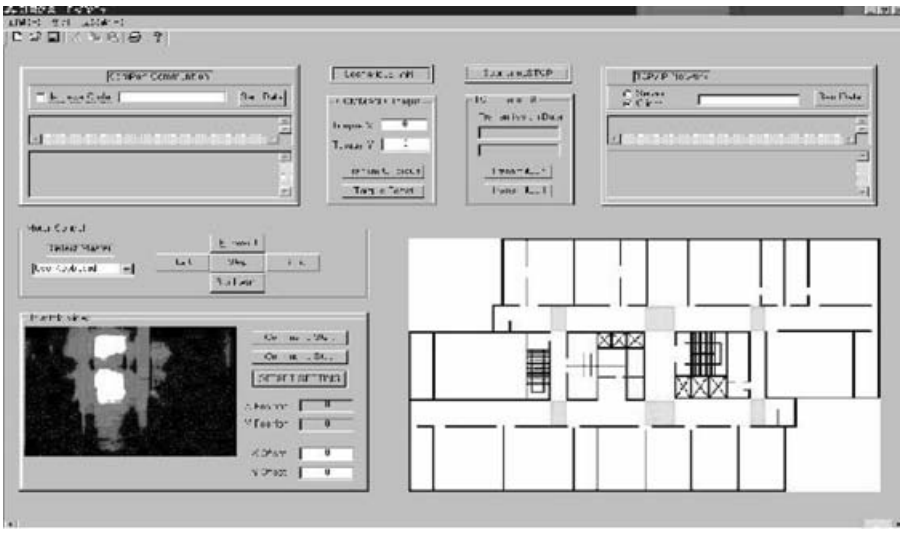


Fig. 14. User interface for tele-operated mobile robot over the Internet.

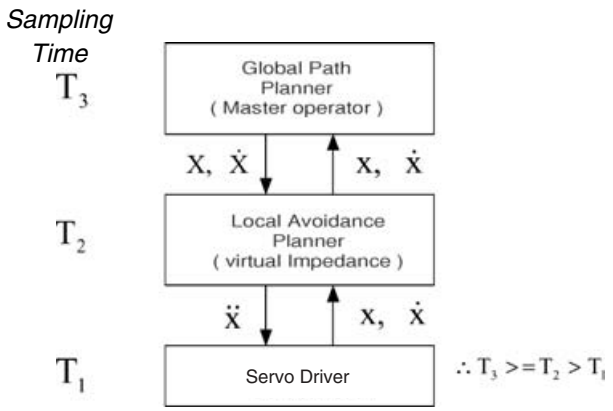


Fig. 15. Sampling time and the control structure of tele-operation system.

displacement through the Internet. Therefore, the velocity of mobile robot is limited to 15 cm/sec.

Figure 16(a)–(f) is the experimental results, captured picture, of obstacle avoidance for mobile robot according to force-reflective joystick control. The virtual force from a mobile robot, which is a new function of the collision vector from 16 ultrasonic sensors, is reflected to the joystick as a force between the joystick and the human hand using two motors in the joystick. The two axial motors are driven by PWM outputs in proportion to the distance detected from collision vector. When a human operator controls the joystick to the direction of near obstacle, he can feel the virtual force in proportion to the distance and then control the joystick to the direction of free obstacles.

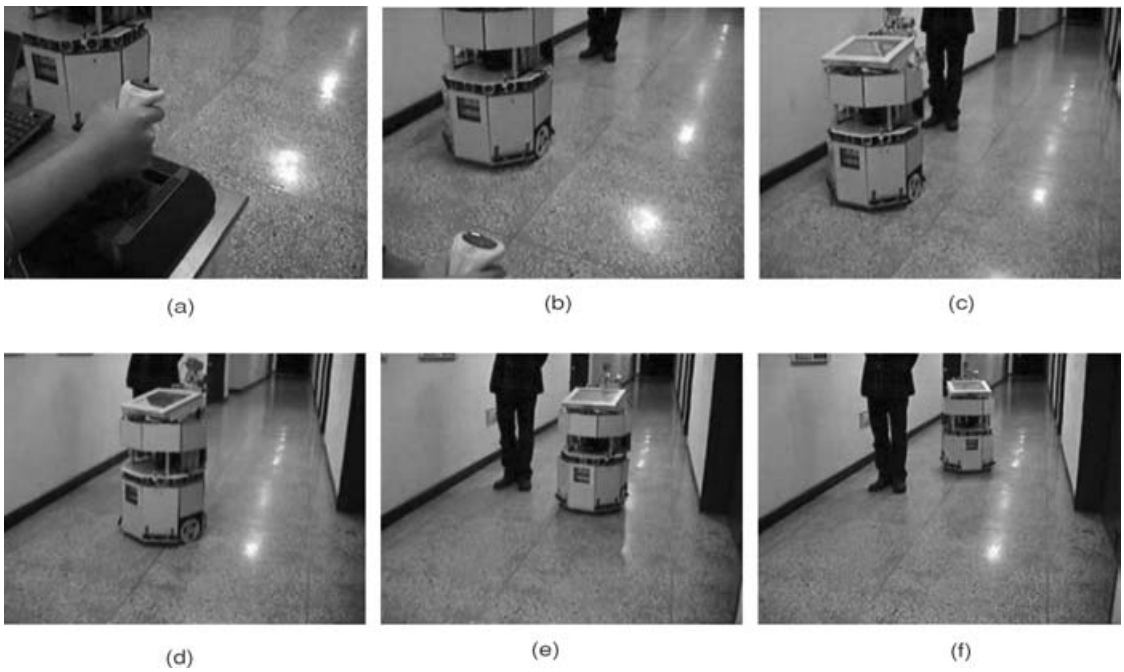


Fig. 16. Experimental result of obstacle avoidance for mobile robot.

https://doi.org/10.1017/S026357470500189X Published online by Cambridge University Press

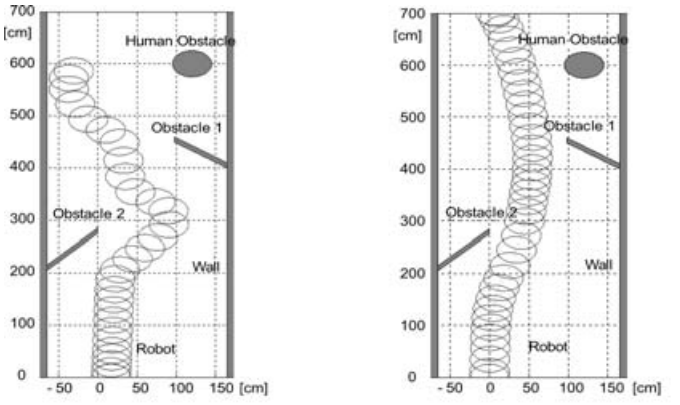


Fig. 17. Experimental results (where $K_r = 2$, $D_r = 10$, $K_0 = 4$, $D_0 = 10$, $M_s = 10$).

The new virtual impedance method is applied to the mobile robot tracking of a given path which avoids obstacles in real time. To validate the effectiveness of force-reflection in the tele-operation of a mobile robot, experiments are performed. Figure 17(a) represents both situation in which the only vision information is reflected to the operator, and the vision and force information are delivered to the operator. Figure 17(b) represents the experimental result when the system combines autonomous obstacle avoidance with the vision and force information is delivered to the operator. At the time, the camera is fixed in the forward-proceeding direction of the mobile robot. As shown by the experimental result in Fig. 17(a), a human tele-operator must exercise extreme care to avoid obstacles in case of using only limited vision information, especially in obstacle-cluttered environments. Consequently, the actual traveling speed of the mobile robot might be very slow. In case of using both vision and force information, a human tele-operator can feel, and avoid, collisions through the joystick in spite of the limitations in visual display, but the mobile robot rocked from side to side, because it is very difficult to examine the actual distance between mobile robot and obstacles through one camera information. The system of autonomous obstacle avoidance with force-reflection can provide an ability of assuming the position and distance of obstacles from the mobile robot in spite of the limitations in visual display. The mobile robot follows the general direction prescribed by the operator. When the robot encounters an obstacle, it autonomously avoids collision with that obstacle, trying to match the operator's prescribed direction as close as possible.

As shown by the comparison of Fig. 17(a) and Fig. 17(b), the latter situation is much safer than the former situation for obstacle avoidance. Although the success of obstacle avoidance is affected by the handling ability of the operator, we obtained similar results in the experiments for three different operators. Figure 18 shows the experimental data obtained for the tele-operation of Fig. 17(b). The first row represents the displacement of the joystick X_m, the second row shows the actual velocities in both directions of a mobile robot, and the last row displays the virtual force feedback to the operator.

V. CONCLUSIONS

A new virtual impedance method that enables a tele-operated mobile robot to follow the desired trajectory while avoiding obstacles in real time, is proposed. In the proposed virtual impedance method, which utilizes a collision vector for obstacle avoidance, the virtual force is generated according

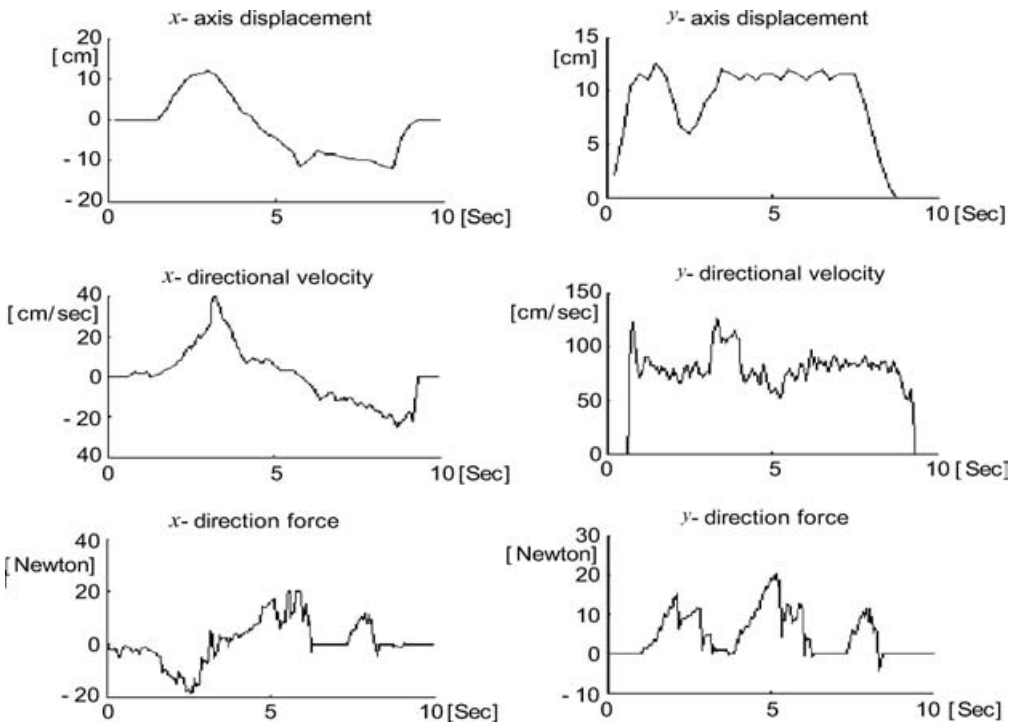


Fig. 18. Master site commands and the feedback force.

https://doi.org/10.1017/S026357470500189X Published online by Cambridge University Press

to both the distance and the approach velocity between obstacles and the robot. This virtual force is reflected to the operator who holds the joystick that converts the force data to the corresponding physical quantities.

The autonomous obstacle avoidance with force-reflective system was implemented and tested successfully on an experimental system. It is shown experimentally that the operator can estimate the position of an obstacle in the remote environment by the virtual force regenerated from the force reflection joystick. That is, in spite of the limited visual information, the operator can feel the spatial sense against the remote environment by using the proposed method. When the robot encounters an obstacle, it autonomously avoids collision with that obstacle, trying to match the operator's prescribed direction as close as possible. Therefore, the teleoperated mobile robot can perform highly skillful tasks in the unstructured environment with an operator who monitors and moves a joystick to generate intelligent commands.

Acknowledgement

This work was supported by "Research Center for Logistics Information Technology (LIT)" hosted by the Ministry of Education & Human Resources Development in Korea.

References

1. J. Borenstein and Y. Koren, "Teleautonomous Guidance for Mobile Robots," *IEEE Trans. on System, Man and Cybernetics* **20**, No. 6, 1437 –1443 (Nov./Dec., 1990).
2. W. Kim, B. Hannaford and A. Bejczy, "Force-reflection and shared compliant control in operating telemanipulators with time delay," *IEEE Trans. on Robotics and Automation* **8**, No. 2, 176–185 (Apr., 1992).
3. D. A. Lawrence, "Stability and Transparency in Bilateral Teleoperation," *IEEE Trans. on Robotics and Automation* **9**, No. 5, 624–637 (Oct., 1993).
4. S. S. Lee and J. M. Lee, "Haptic interface design for the telesurgery," *Proc. of the CIDAM Workshop on Service Automation and Robotics*, Hong Kong (June 19–20, 2000). pp. 81–91.
5. I. Elhajj, N. Xi, W. K. Fung, Y. H. Liu, W. J. Li, T. Kaga and T. Fukuda, "Haptic Information in Internet-Based Teleoperation," *IEEE/ASME Trans. on Mechatronics* **6**, No. 3, 295–304 (Sept., 2001).
6. Y. Zhao and S. L. BeMent, "Kinematics, Dynamics and Control of Wheeled Mobile Robots," *Proc. of IEEE Conf. Robotics and Automation* (May, 1992) pp. 91–96.
7. D. K. Roh, I. M. Kim, B. H. Kim and J. M. Lee, "Localization of a Mobile Robot Using the Information of a Moving Object," *J. of Control, Automation and Systems Engineering* **7**, No. 11, 933–938 (Nov., 2001).
8. J. Borenstein and Y. Koren, "Obstacle avoidance with ultrasonic sensors," *IEEE J. of Robotics and Automation* **RA-4**, No. 2, 213–218 (Apr., 1988).
9. A. Elfes, "Sonar-based real-world mapping and navigation," *IEEE J. Robotics Automation* **RA-3**, No. 3, 249–265 (1987).
10. O. Khatib, "Real Time Obstacle Avoidance for Manipulators and Mobile Robots," *Int. J. Robotics Research* **5**, No. 1, 90–96 (1986).
11. J. Borenstein and Y. Koren, "Real-time obstacle avoidance for fast mobile robots," *IEEE Trans. on System, Man and Cybernetics* **19**, No. 5, 1179–1187 (1989).
12. N. Hogan, "Impedance Control: An Approach to Manipulation, Part I–III," *Transactions of ASME – Journal of Dynamic Systems, Measurement, and Control* **107**, No. 3, 1–24 (1985).
13. T. Arai, H. Ogata and T. Suzuki, "Collision Avoidance Among Multiple Robots Using Virtual Impedance," *Proc. of IEEE/RSJ Int. Workshop on Intelligent Robots and Systems* (Sept., 1989) pp. 479–485.
14. J. Ota, T. Arai, E. Yoshida, D. Kurabayashi and T. Mori, "Real Time Planning Method for Multiple Mobile Robots," *Proc. of IEEE Int. Symposium on, Assembly and Task Planning* (1995) pp. 406–411.

https://doi.org/10.1017/S026357470500189X Published online by Cambridge University Press